DOI: 10.2352/ISSN.2470-1173.2016.19.COIMG-172

Non-uniform Neutron Source Approximation for Iterative Reconstruction of Coded Source Images

Hector J. Santos-Villalobos[1] ***, Jens Gregor***[2] ***, and Philip Bingham***[1]
[1] ***Oak Ridge National Laboratory; Oak Ridge, TN, USA,*** [2] ***University of Tennessee; Knoxville, TN, USA***

Abstract

X-ray and neutron optics both lack efficient ray focusing capabilities. An x-ray source can be made small and powerful enough to facilitate high-resolution imaging while providing adequate flux. This is not yet possible for neutrons. One remedy is to employ a computational imaging technique such as magnified coded source imaging. The greatest challenge associated with successful reconstruction of high-resolution images from such radiographs is to precisely model the flux distribution for complex non-uniform neutron sources. We have developed a framework based on Monte Carlo simulation and iterative reconstruction that facilitates high-resolution coded source neutron imaging. In this paper, we define a methodology to empirically measure and approximate the flux profile of a non-uniform neutron source, and we show how to incorporate the result within the forward model of an iterative reconstruction algorithm. We assess improvement in image quality by comparing reconstructions based respectively on the new empirical forward model and our previous analytic models.

Introduction

Neutron imaging had been mostly employed in the scientific community for Non-Destructive Evaluation (NDE) research. As for X-ray radiography, neutron radiography follows Beer–Lambert Law where the degree of attenuation of a material is proportional to its thickness. However, in contrast to X-rays where the photons interact with the atom electrons, neutron photons interact with the atomic nuclei; making neutrons a complementary imaging modality to X-ray. The strong interaction of neutron photons with molecules that involve hydrogen makes neutron imaging the ideal NDE modality for the assessment and improvement of fuel cell technology [1] and the characterization and modeling of flow on porous and fractured media [2]. Moreover, neutron photons are sensitive to isotope differences and the magnetic field across the traveled path, which makes neutron imaging a valuable interrogation technique for a wide number of applications and research disciplines [1].

In general, neutron radiography is performed on research reactor based facilities, which makes neutron sources virtually non-portable. There are 269 neutron sources world-wide, from which only 116 reactors produce a power greater than 1MW [3, 4], which means most neutron sources are less powerfull than a portable X-ray source. The lack of neutron photon flux makes high resolution imaging at reasonable acquisition times a challenge. Multiple systems have been proposed to overcome this challenge. Wolter optics, or axisymmetric gazing-incidence focusing mirrors, are used to slowly converge neutron rays into a focus point. By employing Wolter optics, the resolution of a traditional setup was increased from $115\mu m$ to $70\mu m$ [5]. The authors also observed a 50 fold increase in flux [6]. The Neutron Microscope is another project aiming to increase spatial resolution beyond $10\mu m$ [7]. A gadolinium oxysulfide screen (Gadox) was used as the scintillator. Although Gadox has greater neutron absorption and resolution when compared to the typical 6LiF/ZnS scintillator, the scintillator produces less light. This drawback is overcome by placing the camera upstream where there is more neutron flux.

Our approach is to employ computational imaging techniques. In particular, we propose to employ coded aperture techniques, where instead of placing a coded mask between object and detector [8, 9, 10], we place the coded mask between source and object–modulating the neutron source [11, 12, 13]. As shown in Figure 1, we select a source-to-object distance much smaller than the object-to-source distance in order to produce magnification and overcome the resolution limitations of a 6LiF/ZnS scintillator, which is around $50\mu m$ [14]. Note that neutron flux and spatial resolution are increased by the total size of the coded mask and with smaller mask sub-apertures, respectively. We call this imaging setup magnified Coded Source Imaging (mCSI).

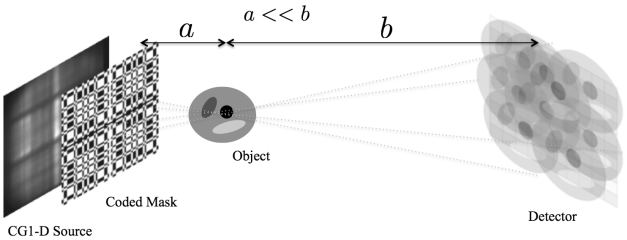

Figure 1. *Relative position of a magnified Coded Source Imaging system in a conventional neutron beam line. Note that each aperture in the coded mask produces a projection of the object at the detector plane.*

In the next section, we provide background technical information about conventional coded source imaging models and reconstruction methods. In the same section, we describe the math-

This manuscript has been authored by UT-Battelle, LLC under Contract No. DE-AC05-00OR22725 with the U.S. Department of Energy. The United States Government retains and the publisher, by accepting the article for publication, acknowledges that the United States Government retains a non-exclusive, paid-up, irrevocable, world-wide license to publish or reproduce the published form of this manuscript, or allow others to do so, for United States Government purposes. The Department of Energy will provide public access to these results of federally sponsored research in accordance with the DOE Public Access Plan (http://energy.gov/downloads/doe-public-access-plan).

DOI: 10.2352/ISSN.2470-1173.2016.19.COIMG-172

ematical formulation of our model-based iterative reconstruction method. In particular, we define the matrix system model and provide a methodology to incorporate into the model the illumination fluctuations typically seen at the ORNL HFIR CG1D neutron imaging beam line. The paper continues with documentation of the synthetic experiments performed to test the proposed flux estimation methodology, and we provide reconstruction results for different configurations. Finally, we close the paper with a summary of the performed work and future directions.

Model-Based Iterative Reconstruction Algorithm

In previous work, we have documented the advantages of a model-based least squares algorithm over direct convolution as well as blind deconvolution wrapped in a maximum-likelihood framework for the reconstruction of coded source radiographs [14]. Using simulated data experiments, we showed that the least squares method outperformed the other methods with respect to image quality and reconstruction precision as a result of the modeling of the system components, such as the neutron source, the distribution of flux through the detector pixels, the system field of view, imperfections of the coded mask, etc. [14] However, these experiments were limited to uniform and Gaussian neutron sources which, as shown in Figure 2, do not represent real life neutron sources. We argue that the greatest challenge associated with successful reconstruction of real data from a complex source such as the HFIR CG-1D is to precisely model the neutron rays flux distribution at each coded mask hole.

System Model

Under a far field assumption, encoded radiograph P can be modeled as the convolution of object O, coded aperture A and the addition of random noise η:

$$P = O * A + \eta. \tag{1}$$

Coded aperture imaging techniques apply to mCSI, consequently, coded aperture patterns such as Modified Uniformly Redundant Array (MURA) and deconvolution reconstruction approaches [15, 16] can be seamlessly employed in CSI. Deconvolution by a properly defined kernel G can be used to determine O given A and P [14]. When P is corrupted by additive noise η, as is typically the case, the object must be imaged a second time using a complementary aperture mask $\bar{A}$, where the apertures in A are closed in the complementary mask and vice-versa, with the exception being that the central aperture remains closed or zero for both $\bar{A}$ and A [17]. Using "mask-antimask" imaging, the object can be reconstructed as

$$\begin{aligned}\hat{O} &= \frac{1}{2}(P_A - P_{\bar{A}}) * G \\ &= \frac{1}{2}(O * A + \eta - (O * \bar{A} + \eta)) * G \\ &= \frac{1}{2}(O * (A * G) + O * (\bar{A} * -G)) \\ &= O.\end{aligned} \tag{2}$$

However, this model holds only if the neutron illumination source uniformly emits rays parallel to the imaging axis, A and $\bar{A}$ are perfectly aligned and free of manufacturing imperfections, and that the system point spread function $A * G = \delta$ [14]. These requirements are not met in a magnification modality, where near-field imaging and divergent rays are needed. In addition, the flux distribution of an actual neutron source is far from ideal.

When taking a model-based approach to solving the inverse problem of reconstructing O, the beam and its interaction with first the coded aperture A and then the object O must be captured by the so-called system model. Consider the following discretization. Let A_n denote the aperture state at the n^{th} point of the coded aperture; assign a one to A_n if the mask has an opening and a value of zero if the mask blocks the beam. Let P_m denote the m^{th} point of the detector, and let O_q denote the transmission through the q_{th} point of the object (which we treat as a uniform slab). The ray that connects A_n and P_m intersects the object somewhere in the vicinity of O_q. We have previously reported on using bi-linear interpolation coefficients $c_{n,m,q}$ to weight the transmission contribution of this point and its neighbors [18]. Then, we can define the neutron flux for the ray $< m,q >$ as

$$w_{m,q} = \sum_{n=1}^{N} A_n c_{n,m,q} \Phi_{n,m,q}, \qquad m \in [1,M], \qquad q \in [1,Q]$$

where $\Phi_{n,m,q}$ is the probability of a neutron particle passing through mask hole A_n, detector pixel m and object pixel q. Note that for a uniform neutron source the flux term is constant $\Phi_{n,i,j} = \Phi$. For non-uniform sources where all coded aperture mask holes have an equivalent flux angular distribution (e.g., Gaussian source), the flux term is redefined as $\Phi_{n,i,j} = \Phi_{i,j}$, where the tuple i, j index the angular flux variation. Shortly, we will discuss how we estimate $\Phi_{n,i,j}$ for the HFIR CG1-D neutron source. This allowed the relationship between the source, the aperture mask, the object and the detected data to be modeled by the linear system

$$WO = P \tag{3}$$

where

$$W = \begin{bmatrix} w_{1,1} & \cdots & w_{1,Q} \\ \vdots & \ddots & \vdots \\ w_{M,1} & \cdots & w_{M,Q} \end{bmatrix}, \qquad O = \begin{bmatrix} O_1 \\ \vdots \\ O_Q \end{bmatrix}, \qquad P = \begin{bmatrix} p_1 \\ \vdots \\ p_M \end{bmatrix}$$

A simpler system model could be based on using the nearest neighbor instead of carrying out the bi-linear interpolation. However, as the computational savings are negligible and the resulting images are of lower quality, we do not consider this as a viable option. In this paper, we instead use a computationally costlier system model which we have found to produce images of higher quality. This model is based on the area intersection of the beam with the pixels. The four corners of the pixelated source are connected to the four corners of the detector pixels. This defines a bounding box in the image plane. The above c-coefficients are in turn redefined as intersection probabilities computed as the ratio of the area of the pixel covered by the bounding box and the area of the bounding box itself.

The typical system matrix W is not square or invertible. Therefore, we instead solve Equation (3) indirectly using the so-called SIRT (Simultaneous Iterative Reconstruction Technique) algorithm [19] which implements a gradient decent for the

DOI: 10.2352/ISSN.2470-1173.2016.19.COIMG-172

weighted least-squares problem $\|WO-P\|_R^2$ preconditioned by C where R and C are diagonal matrices of inverse row and column sums of system matrix W, respectively. The update equation is given by:

$$\hat{O}^{k+1} = \hat{O}^k + \alpha C W^T R \left(W \hat{O}^k - P \right). \quad (4)$$

Relaxation parameter α controls the convergence rate; $\alpha = 1.99$ has been shown to be a near-optimal choice. The experimental results reported below are based on $\hat{O}^0 = 0$ but other initializations are possible. Tikhonov based regularization is easily added to ensure uniqueness and/or produce a smooth solution. SIRT was recently shown to be comparable to SQS (Separable Quadratic Surrogates) when using such quadratic regularization [20].

Shortly, we discuss the methodology for the empirical estimation of neutron source flux $\Phi_{n,m,q}$. In order to quantitatively compare the resulting source model approximation with ground truth, we have added the ability to import Monte Carlo generated list-mode data. This allows us to construct the system model using simulated data in the form of a vast number of source rays given by mask and detector coordinates which are converted to bi-linear interpolation coefficients that can be applied to image and detector pixel indices. The reconstruction results from the approximated system matrix are assessed against this ideal system matrix computed directly from Monte Carlo neutron traces.

Empirical estimation of $\Phi_{n,m,q}$

Conventional coded aperture algorithms assume the source is parallel and uniform. Although methodologies to compensate for angular non-uniformities exist, these techniques cannot be applied to the HFIR CG1-D beam where the source also varies spatially. As shown in Figure 2(a), the neutron hits at the detector produce significant variations in intensity and these high frequency features change with the viewpoint due to the curved construction of the neutron guide that allow neutrons generated at source reach the imaging station.

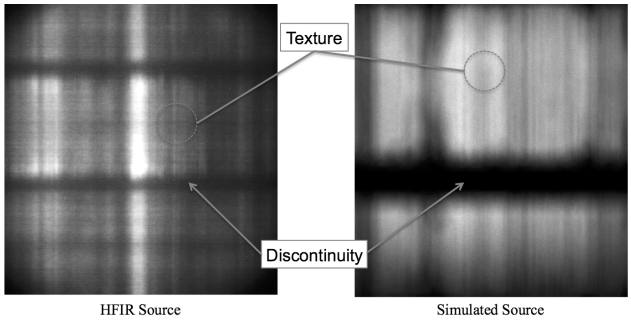

Figure 2. *Illustration of real and simulated neutron sources imaged with a 2mm pinhole: at the left is the HFIR CG1D neutron source and at the right is our simulation of the HFIR source with McStas.*

We account for the corresponding variations in flux by using a collection of source images obtained using a grid of small apertures, named characterization apertures. By choosing an odd number of grid points, such as 3×3 or 9×9, we ensure that a central view is included corresponding to what was used previously for the single view source model. The multi-view source contribution to the system model is calculated by applying bi-linear interpolation to the four nearest source views for a given ray, as illustrated in Figure 3. The flux distribution is given by

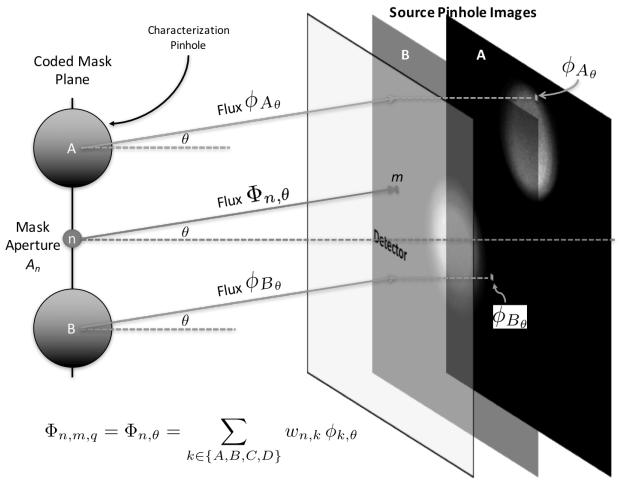

Figure 3. *Side view illustration of source flux estimation from empirical samples. The flux for aperture n is approximated by computing the weighted average of the intensity of the neighbor characterization sources open beam projections. The open beam radiographs for characterization apertures A and B are at the same detector plane, they are shown at different depths for illustration purposes.*

$$\Phi_{n,m,q} = \Phi_{n,\theta} = \sum_{k\in\{C_{UL},C_{UR},C_{BL},C_{BR}\}} \omega_{n,k} \times \phi_{k,\theta},$$

where θ is the direction of the ray passing through detector and object pixels m and q, respectively. The weights ω_k sum to 1 and ω_k is inversely proportional to the distance between the mask aperture A_n and characterization apertures $k \in C_{UL}$,C_{UR}, C_{BL}, C_{BR}. Then, $\phi_{k,\theta}$ is the intensity of the pixel that correspond to the direction θ for the open beam projection of the characterization source k. Note that the same source characterization images can be used for different mask and objects as long as the mask position remains unchanged and the mask size fit inside the outer characterization apertures.

The choice size and placement of the characterization apertures will determine the accuracy of the estimation of the flux function $\Phi_{n,m,q}$. For example, small aperture sizes, such as $254\mu m$ will resolve small variations in flux, but may require a larger set of characterization apertures across the coded aperture plane. On the other hand, larger aperture sizes, such as the $1mm$ aperture, may reduce the number of characterization apertures needed across the coded mask plane, but will smooth the actual flux values. The experiments below aims to define which characterization configuration provides the optimal estimate of $\Phi_{n,m,q}$ by number and size of the characterization apertures.

HFIR CG1D Simulations and System Configuration

Neutron imaging beam lines user facilities are in high demand and the allocated beam time is limited to a couple to three days at a time. Therefore, we needed to find an alternate route to test the performance of the reconstruction method. In particular, we wanted to determine what is the ideal configuration for

DOI: 10.2352/ISSN.2470-1173.2016.19.COIMG-172

the characterization sources in order to estimate the flux distribution of the HFIR CG1D source. Consequently, we implemented a ray tracing model of the beam line in McStas [21]. The right image in Figure 2 shows the Monte Carlo ray tracing result of our synthetic model and imaging with a 2mm pinhole. The difference between the left and right images in Figure 2 is due to different magnification setup. What is relevant to our experiment is that we were able to generate a texture and discontinuities similar to those found in the real sources. Similarly to the actual neutron source, moving the position of the pinhole change the texture pattern on the projection.

The configuration of CSI system is shown in Figure 4. We use a MURA coded pattern with 57×57 $100\mu m$ apertures. For a test object, we employed a 1024×1024 $29\mu m$ pixels Sheep-Logan Phantom typically used for testing of X-ray Computed Tomography reconstruction algorithms. The size of the phantom pixels was selected such that the main phantom features appear inside the $2mm$ field-of-view aperture. The detectors has an area of 701×701 $50\mu m$ pixels. The distance from coded aperture to object is 1 meter and the distance from object to detector is 4 meters. This produces an effective object magnification of $5x$. The left image in Figure 5 shows an actual projection of the phantom when imaged with the $100\mu m$ MURA coded mask. Note that the phantom is not perceivable in the projection.

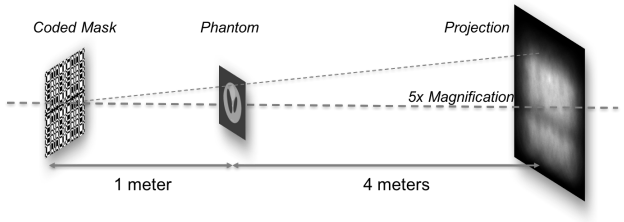

Figure 4. *Illustration of coded source imaging configuration.*

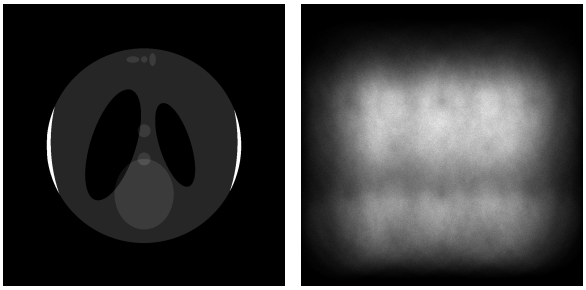

(a) (b)

Figure 5. *(a) Low contrast Sheep-Logan phantom used in Monte Carlo simulations. (b) Coded source projection of phantom object.*

For the characterization sources, we tested seven different source characterization grid patterns, 1×1, 3×3, 5×5, 9×9, 13×13, 23×23, 45×45. For each grid pattern, the characterization sources are distributed uniformly in a $5.7mm \times 5.7mm$ area, with the center characterization source align with the z-axis of the beam line, as it is the case for the coded aperture, phantom, and detector. Three characterization aperture sizes were tested $254\mu m$, $500\mu m$, and $1mm$. Projection images without the phantom in place were simulated for each characterization aperture position and size. These images were later utilized by the reconstruction algorithm to estimate the flux of the neutron sources using the methodology described above.

Reconstruction Results

As shown in Figure 6(a), direct deconvolution reconstruction with a single mask is negatively impacted by the nonuniform illumination of the CG1-D source. The reconstructed image suffers from illumination fluctuations and low contrast. Figure 6(b) shows convolution-based reconstruction results when the object is imaged with both the mask and the anti-mask. Although this reconstruction has better quality than the reconstruction in Figure 6(a), this reconstruction falls short from the desired image quality and the intensity values do not match the actual attenuation values in the phantom. Also, recall that the mask/anti-mask convolution-based method requires an additional image capture with an accurately registered anti-mask. This becomes a challenge when trying to image with mask apertures smaller than $10\mu m$. Therefore, it is preferred to image the object with a single mask in order to remove artifacts introduced by miss-registration of high resolution coded apertures. Moving towards that goal, the model-based reconstruction algorithm should provide superior quality by integrating in the model non-idealities, such as source non-uniform illumination, mask manufacturing defects and transparency, and mask, object, and detector misalignments. Figure 6(c) shows model-based reconstruction result with a single mask and with the system matrix computed from actual Monte Carlo neutron traces. Consequently, the utilized system matrix is a perfect model for the imaging system. The reconstruction shows sharp edges and the appropriate attenuation values for the imaged phantom. The reconstruction is our baseline to assess the image quality of reconstructions with an approximated system model using the flux estimation method above.

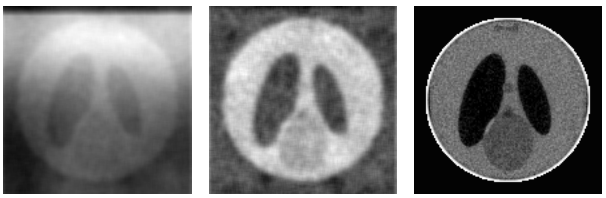

(a) (b) (c)

Figure 6. *(a) Convolution-based reconstruction when object imaged with the aperture mask alone. (b) Convolution-based reconstruction when object imaged with both aperture and anti-aperture. (c) Model-Based reconstruction using the aperture mask and the ideal system matrix.*

Figure 7 shows the best reconstructions obtained using the flux approximation method. The reconstruction are not as sharp and detailed as the with the reconstructions with the ideal system matrix (Figure 6(c)). However, reconstructions with the approximated system matrix compares to reconstructions with the mask-anti-mask convolution-based method (Figure 6(b)). Although, the contrast for the convolution-based and model-based methods is comparable, the model-based method outperform the other method by producing attenuation values that closely resemble those found in the phantom. Some of the artifacts found in the best model-based reconstruction may be attributable to low

DOI: 10.2352/ISSN.2470-1173.2016.19.COIMG-172

statistics at the projection image.

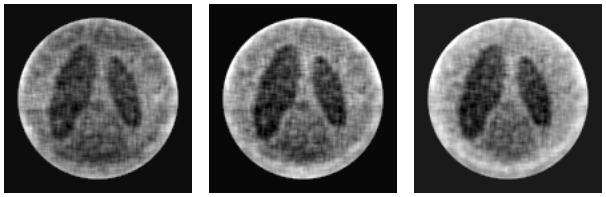

(a) (b) (c)

Figure 7. *Reconstructions for the* 254μ*,* $500\mu m$*, and* $1000\mu m$ *characterization aperture for grid sizes (a)* 45×45*, (b)* 23×23*, and (c)* 13×13*, respectively*

One of the goals of this investigation was to define an adequate grid size and spacing for the characterization sources. Figure 8 shows the Root Mean Square Error (RMSE) curves for the difference between the ideal and approximate system matrices as a function of grid size. Each plot lines corresponds to a characterization source aperture size. The horizontal axis relates to the grid size used to sample the coded mask plane in order to estimate flux. Source flux estimation with grid sizes smaller than 5×5 produced poor reconstruction results. We only show worst case reconstructions for the $1mm$ pinhole (See Figure 9(a)). Similar results were obtained for the smaller characterization source apertures. Note that for the $1mm$ characterization aperture, the reconstructions start to resemble the phantom for grid sizes larger than five (Figure 9(b)). For smaller apertures, a larger grid size was required in order to achieve a reconstruction that partially showed the phantom. Also, when comparing Figure 7(c) to Figure 9(c), we observed that after the spatial sampling of the coded mask area reaches a certain density, improvement of reconstruction quality is minimal.

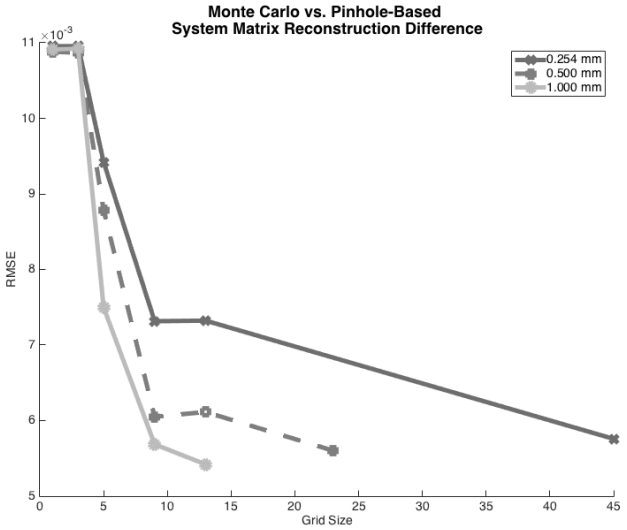

Figure 8. *RMSE curves between the ideal reconstruction in Figure 6(c) and the reconstructions using the characterization sources to estimate* $\Phi_{n,m,q}$

Our synthetic experiments confirms the high frequency textures introduced by the neutron guide. These textures change quickly with slight modifications to the point of view. Figure 10 shows the same error measurements from Figure 8, but this time the horizontal axis relates to the ratio between source characterization spacing and size. As the ratio reaches infinity, i.e., less spatial sampling, the reconstruction algorithm is unable to recover the object. For a $1mm$ characterization source and a grid size of 13×13, the center-to-center spacing is $0.457mm$. This is half the size of the characterization source, therefore, there is a slight overlapping between the characterization sources. The same observation is repeated for the $254\mu m$ and the $500\mu m$ characterization apertures for grid sizes 23×23 and 45×45, respectively. Consequently, the best reconstruction quality is obtained when the aperture spacing/size ratio is around 50%. Note that image quality did not increase for smaller apertures at the same characterization source spacing/size ration. This may be due to the higher frequency details resolved by the smaller apertures that are more difficult to approximate by interpolation. A larger characterization source, trades a more accurate sample of the source flux for a smoother flux function to interpolate.

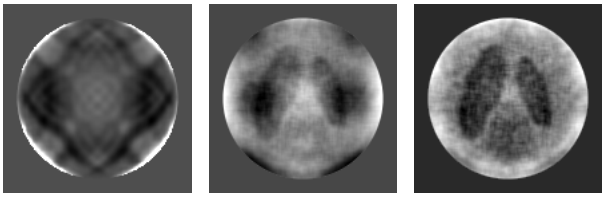

(a) (b) (c)

Figure 9. *Reconstructions for* $1mm$ *characterization aperture for grid sizes (a)* 3×3*, (b)* 5×5*, and (c)* 9×9

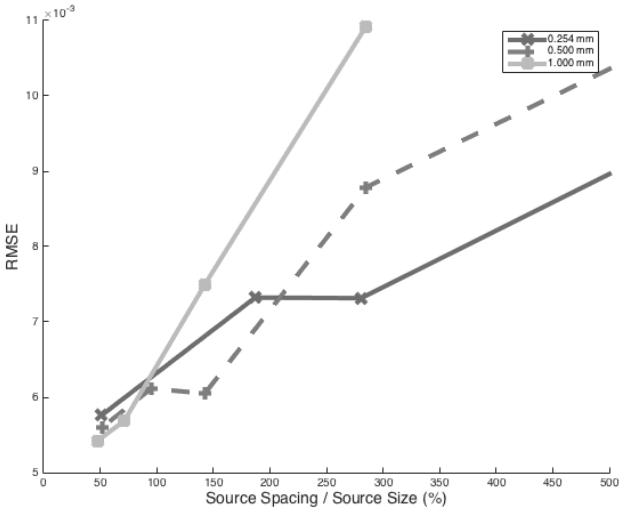

Figure 10. *Same RMSE analysis from Figure 8 as a function of characterization source spacing and size.*

Conclusion

The ORNL's HFIR CG1D neutron imaging beam line produces high frequency textures that are introduced by the structure of the neutron guide. Both spatial and angular flux intensities change rapidly with point of view. When developing a model-based iterative reconstruction technique, this fluctuations in flux becomes a modeling challenge, because the flux is difficult to estimate. We had documented a methodology to estimate the flux profile of a neutron imaging beam line, such as the HFIR CG1D.

DOI: 10.2352/ISSN.2470-1173.2016.19.COIMG-172

We image the neutron source with pinholes, which we call characterization source apertures, at different locations in order to obtain a set of flux samples that we can integrate into the reconstruction system model. The preliminary, synthetic results show an improvement over convolution-based method. In particular, we show that the model-based iterative method yields equivalent reconstruction results without the need of a second image capture with a complementary mask as is needed for the convolution-based mask-anti-mask method. The low contrast and artifacts on current reconstructions can be due to the low statistics at the detector. We plan to extend this study to additional coded mask aperture sizes in order to investigate the relationship between reconstruction quality, coded mask hole size, and the characterization sources size and sampling pattern.

Acknowledgment

Funding for this effort came from the U.S. Department of Energy through an early career award out of the Office of Basic Energy Sciences which also sponsors both the High Flux Isotope Reactor and the Center for Nanophase Materials Sciences at Oak Ridge National Laboratory where portions of this research were performed.

References

[1] N. Kardjilov, I. Manke, and A. Hilger, M. Strobl, and J. Banhart, Neutron imaging in materials science, Materials Today, 14, 248 (2011).

[2] P. Bingham, Y. Polsky, L. Anovitz, J. Carmichael, H. Bilheux, D. Jacobsen, and D. Hussey, Neutron Radiography of Fluid Flow for Geothermal Energy Research, Proc. 10th World Conference on Neutron Radiography, pg. 464. (2014).

[3] E. Lehmanna and D. Ridikas, Status of Neutron Imaging - Activities in a Worldwide Context, Proc. 10th World Conference on Neutron Radiography, pg. 10. (2014).

[4] M. J. Paulus, S. S. Gleason, S. J. Kennel, P. R. Hunsicker, and D. K. Johnson, High Resolution X-Ray Computed Tomography: An Emerging Tool for Small Animal Cancer Research, Neoplasia, 2, 62, (2000).

[5] D. Liu, D. Hussey, M. Gubarev, B. Ramsey, D. Jacobson, M. Arif, D. Moncton, and B. Khaykovich, Demonstration of Achromatic Cold-Neutron Microscope Utilizing Axisymmetric Focusing, Applied Physics Letters, 102, 183508 (2013).

[6] B. Khaykovich, M. Gubarev, D. Liu, B. Ramsey, and D. Moncton, A New Generation of Neutron-Focusing Optics, SPIE Newsroom Optical Design & Engineering, (2014).

[7] E. Lehmann and W. Wagner, Neutron Imaging at PSI: A Promising Tool in Materials Science and Technology, Applied Physics A, 99, 627 (2010).

[8] A. Busboom, H. D. Schotten, and H. Elders-Boll, Coded Aperture Imaging With Multiple Measurements, J. Opt. Soc. Am. A, 14, 1058 (1997).

[9] E. Caroli, J. Stephen, G. Cocco, L. Natalucci, and A. Spizzichino, Coded Aperture Imaging in X- and Gamma-Ray Astronomy, English Space Science Reviews, 45, 349 (1987).

[10] E. Fenimore and T. M. Cannon, Coded Aperture Imaging With Uniformly Redundant Arrays, Applied Optics, 17, 337 (1978).

[11] A. L. Damato, B. K. P. Horn, and R. C. Lanza, Coded Source Imaging for Neutrons and X-Rays, IEEE Nuclear Science Symposium Conference, pg. 199. (2006).

[12] M. Schulz, P. Böni, E. Calzada, M. Mühlbauer, and B. Schillinger, Energy-Dependent Neutron Imaging With a Double Crystal Monochromator at the ANTARES Facility at FRM II, Nuclear Instruments & Methods in Phys. Research A, 605, 33 (2009).

[13] P. Bingham, H. Santos-Villalobos, and K. Tobin, Coded Source Neutron Imaging, SPIE Machine Vision Applications IV, pg. 7877. (2011).

[14] H. Santos-Villalobos, P. Bingham, and J. Gregor, Iterative Reconstruction of Coded Source Neutron Radiographs, IEEE Transactions on Nuclear Science, 60, 1624 (2013).

[15] S. Gottesman and E. Fenimore, New Family of Binary Arrays for Coded Aperture Imaging, Appl. Opt., 28, 4344 (1989).

[16] K. Byard, Square Element Anti-Symmetric Coded Apertures, Experimental Astronomy, Springer Netherlands, 2, 227 (1992).

[17] R. Accorsi and R. Lanza, Near-Field Artifact Reduction in Planar Coded Aperture Imaging, Applied Optics, 40, 4697 (2001).

[18] H. Santos-Villalobos, P. Bingham, J. Gregor, Iterative Reconstruction of Coded Source Neutron Radiographs, IEEE Nuclear Science Symposium and Medical Imaging Conference, pg. 968. (2012).

[19] J. Gregor and T. Benson, Computational Analysis and Improvement of SIRT, IEEE Trans. Medical Imaging, 27, 918 (2008).

[20] J. Gregor and J.A. Fessler, A Comparison of SIRT With SQS for Regularized Weighted Least Squares Image Reconstruction, IEEE Trans. Computational Imaging, 1, 44 (2015).

[21] K. Lefmann and K. Nielsen, McStas, A General Software Package for Neutron Ray-tracing Simulations, Neutron News, 10, 20 (1999).

Author Biography

Dr. Hector J. Santos-Villalobos is an R&D Staff member of the Imaging, Signals, and Machine Learning Group (ISML) at the Oak Ridge National Laboratory since 2012. He received B.S. and M.S. degrees in 2003 and 2005, respectively, from the Department of Computer and Electrical Engineering at the University of Puerto Rico. In 2010, he received a Ph.D. from the School of Electrical and Computer Engineering at Purdue University and right after, he joined the ISML group as a post doctorate student. During his time at ORNL, he has worked on a variety of imaging modalities and some of his key project areas are biometrics, coded aperture imaging, plenoptic imaging, and elastic ultrasound imaging.

Dr Jens Gregor received a PhD in Electrical Engineering from Aalborg University, Denmark in 1991. Following graduation, he joined the faculty at the University of Tennessee, Knoxville, where he currently holds the rank of Professor in the Department of Electrical Engineering and Computer Science. His research, which focuses on pattern recognition and computed imaging, has been published in a total of more than 85 book-chapters, journal articles and conference papers.

Dr Philip Bingham received a Phd and MS in Electrical and Computer Engineering (ECE) from the Georgia Institute of Technology and a BS in ECE at the University of Tennessee. He has been a member of the Imaging, Signals, and Machine Learning group at Oak Ridge National Laboratory for 16 years and is currently the group leader. His research interests lie in applied computational imaging.